Mechanism of subwavelength imaging with bilayered magnetic metamaterials: Theory and experiment

O. Sydoruk
Department of Physics, University of Osnabrück, D-49069 Osnabrück, Germany

M. Shamonin
Department of Electrical Engineering and Information Technology, University of Applied Sciences, D-93025 Regensburg, Germany

A. Radkovskaya
Magnetism Division, Faculty of Physics, M. V. Lomonosov Moscow State University, Leninskie Gory, Moscow 119992, Russia

O. Zhuromskyy and E. Shamonina[a]
Department of Physics, University of Osnabrück, D-49069 Osnabrück, Germany

R. Trautner
Department of Electrical Engineering and Information Technology, University of Applied Sciences, D-93025 Regensburg, Germany

C. J. Stevens, G. Faulkner, and D. J. Edwards
Department of Engineering Science, University of Oxford, Parks Road, Oxford OX1 3PJ, United Kingdom

L. Solymar
Optical and Semiconductor Devices Group, Electrical and Electronic Engineering (EEE) Department, Imperial College, Exhibition Road, London SW7 2BT, United Kingdom

We present a theoretical and experimental study of a bilayered metamaterial structure for subwavelength imaging of magnetic field. The simplest version of such a structure consists of one or two linear arrays of capacitively loaded split pipe resonators. Its subwavelength physics is governed by strongly anisotropic magnetic coupling between individual resonators and by propagation of magnetoinductive waves with wavelength much shorter than the wavelength of the electromagnetic radiation in free space. It is shown that magnetoinductive waves propagating in the lateral direction are undesirable because they spread the image. Good subwavelength imaging is achieved when, due to the strong interlayer coupling, a stop band in the vicinity of the resonant frequency appears in the dispersion characteristics. The imaging properties of the single and double lens are compared and it is shown that the double lens has a superior performance. Excellent agreement is obtained between experimental and theoretical results for the magnetic field in the image plane in the operation frequency range of 30–60 MHz. It is shown that the same mechanism is responsible for image formation using bilayered planar metamaterial structures and a design of such a lens comprising two planar layers with a total of 542 elements is provided. The conclusions are not restricted to the radio frequency region because the elements can be scaled down. © *2007 American Institute of Physics*. [DOI: 10.1063/1.2714782]

I. INTRODUCTION

The seminal paper by Pendry[1] on the possibility of subwavelength imaging using a slab with negative refractive index, $n < 0$, triggered an upsurge of interest in the field of metamaterials. Pendry argued that a material with $n = -1$ would serve as a perfect lens for two different kinds of reasons. The first reason for perfect imaging is negative refraction of the propagating components at both surfaces of the metamaterial slab. The divergence in the air is compensated by convergence within the slab. However, for the slab to act as a perfect lens, that is to be able to produce an image also for a subwavelength object, a flat transfer function is required for all spatial frequencies which constitute the near-field of the object. Thus the key to the perfect lens lies in the fact that the evanescent components, which decay in air, must grow inside the metamaterial slab so that the decay and the growth just compensate each other resulting in a flat transfer function.

Pendry also suggested that for an object with TM polarization it is sufficient to use a slab with negative permittivity only, $\varepsilon < 0$, so that the permeability may remain positive. He proposed silver as the material which has the required negative permittivity below its plasma frequency in the ultraviolet at 360 nm. At this frequency the excitation of surface resonant modes of Plasmon polaritons provides the mechanism for the amplification of the evanescent components. It is essential that surface modes (decaying exponentially away

[a] Author to whom correspondence should be addressed; electronic mail: ekaterina.shamonina@uos.de

from each surface) are excited on both surfaces. These coupled modes are better pronounced in a thinner slab[2] resulting in two well-separated spatial resonances with a flat transfer function for spatial components of the spectrum in between. For a finer image thinner slabs are required. If it is desirable for the image to be transferred over a larger distance, the solution is offered in the form of a multilayered lens made from a series of thinner slabs with negative permittivity separated by thin layers with positive permittivity.[2] Recent experimental evidence of this idea was provided by Melville and Blaikie.[3]

It is worth mentioning that the picture of purely growing evanescent waves within the slab with $\varepsilon < 0$ is oversimplified. Only for a certain part of the spatial frequency spectrum, when the rear-surface resonance is strong, is it true that the field appears to decay exponentially in the backward direction from the rear surface toward the front surface which appears as an exponential growth in the forward direction. Generally both surfaces, the front one and the rear one, exhibit resonances so that the field distribution is a superposition of exponential functions decaying to both sides from both surfaces. This has already been pointed out in Ref. 4 and, more recently, in Ref. 5.

Ever since Pendry's paper on the perfect lens the idea of near-field imaging has been a driving force in the rapid development of the field of metamaterials as the search for suitable structures capable of near field imaging continues. A large variety of physical mechanisms was suggested to be responsible for near field imaging, ranging from effective medium theory[6] and excitation of surface plasmon-polariton resonances[7] to imaging based on the curvature of the dispersion characteristics (see, e.g., Ref. 8), phase conjugation,[9] or propagation of magnetoinductive (MI) waves.[10]

Using a direct analogy between the phenomenon of negative refraction and phase conjugation, Maslovski and Tretyakov[9] proposed an alternative device for perfect imaging. They showed that a metamaterial slab with $n=-1$ is mathematically equivalent to two phase conjugating planes in free space. Phase conjugating interfaces also lead to both negative refraction of propagating components and to surface resonances for evanescent components resulting in the restoration of the near-field part of the object spectrum. Similar ideas were also proposed by Allen *et al.*[11] and Lin *et al.*[12]

The idea that the resonant excitation of coupled surface modes is essential for near field imaging was further developed by Maslovski *et al.*[7] They argued that any system of two coupled planar material sheets possessing surface modes of polariton resonances can be used for the purpose of evanescent field restoration and thus for subwavelength near field imaging. As an example, realized at microwaves, two grids of weakly interacting resonant particles in the form of meandered copper wire were used. The essential features of the device are that, at the imaging frequency, the rear grid of particles is being excited stronger than the front grid and that weak interactions between the particles within each layer do not lead to spreading of the field distribution from the source.

An alternative method of subwavelength imaging via the regime of "canalization"[8] is based on the curvature of the dispersion characteristics. This method does not involve negative refraction and amplification of evanescent modes. Instead, most part of the spatial spectrum of the source radiation is transformed into propagating eigenmodes of the structure with the same longitudinal components of the wave vector. The spatial harmonics of the object, both propagating and evanescent, refract into the crystal eigenmodes at the front surface. These eigenmodes propagate normally to the interface and deliver the distribution of near-field electric field from the front surface to the rear surface with little disturbance. Then the waves refract at the rear surface and form an image. Belov *et al.* proposed to employ a medium of capacitively loaded wires aligned parallel to the front and the rear and concluded that subwavelength resolution up to $\lambda/6$ is achievable. The approach of making use of the curvature of dispersion characteristics for manipulating near field properties was used since the 1970s, e.g., by Silin,[13–15] Zengerle,[16] and by Smith *et al.*[17] A variety of names for similar regimes of near field imaging were proposed which include self-guiding,[18] directed diffraction,[19] self-collimation,[20] and tunneling.[21]

Experimentally, the so-called Swiss roll lens (a single layer of resonant Swiss rolls), was shown to be able to transfer subwavelength information from the object to the image plane.[6,22] The "pixel-to-pixel" imaging principle was also employed on a different device, an array of parallel conducting wires aligned perpendicular to the front and rear surfaces.[23] Explanations of imaging with a single layer of Swiss rolls in Refs. 22, 24, and 25 were based on the existence of a negative permeability region. A competing explanation proposed in Ref. 26 is based on the microscopic description of the subwavelength physics of the structure. It takes into account the strong magnetic coupling between individual elements which leads to the propagation of slow MI waves. The presence of MI waves in a two-dimensional layer of Swiss rolls was shown to lead to strong distortion of the image. This theoretical description fully matched experimental observations by Wiltshire *et al.*[24] who demonstrated that imaging is not possible in the vicinity of the resonant frequency where a series of spatial resonant modes were excited that prevented the pixel-to-pixel transmission and distorted the observed picture.

Freire and Marques proposed to use a two-layered structure of split ring resonators for the near-field imaging suggesting that when the structure consists of two parallel planes of magnetic metamaterial elements then MI waves may play a positive role[10] resulting in growing fields in the inter-layer spacing. Our aim is to investigate in more detail, both theoretically and experimentally, the imaging mechanism for bi-layered magnetic metamaterials. In order to perform a simple analysis of how a near-field magnetoinductive lens works we start with a simpler case of a bilayered configuration when the lens consists of either one or two linear arrays parallel to each other. Our theoretical model is based on a coupled-mode approach for magnetoinductive waves. The theoretical predictions are confirmed by experimental results in the range of 30–60 MHz on structures operating at frequencies around 46 MHz. We then design a bilayered planar metama-
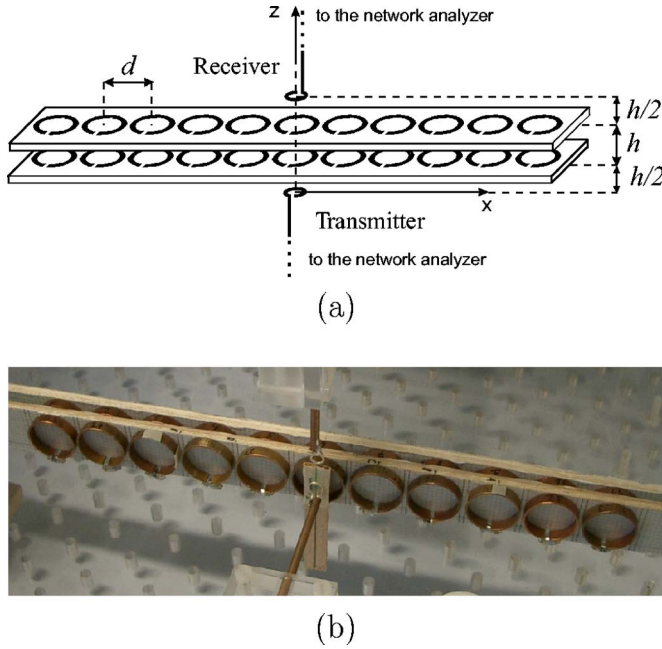
FIG. 1. (Color online) Schematic presentation of the two-layer magnetoinductive lens (a) and photograph of the experimental setup (b).

terial comprising 542 elements arranged hexagonally in each layer and show that the same mechanism is responsible for the subwavelength image formation.

The structure of the paper is as follows. The analytical model of coupled linear arrays is discussed in Sec. II. Experimental and theoretical results for the linear near-field lens are shown in Sec. III. Comparison of the imaging capabilities of a double lens with those of a single lens is performed in Sec. IV. The model is applied for the design of a bilayered planar magnetic metamaterial in Sec. V. Conclusions are drawn in Sec. VI.

II. MAGNETOINDUCTIVE LENS AS A BIATOMIC METAMATERIAL

A. Dispersion characteristics

A schematic representation of the imaging device in its simplest form of two planar arrays parallel to each other (double lens) is shown in Fig. 1(a). For a practical realization see Fig. 1(b). The single lens was obtained by omitting one of the layers from the double lens. The elements are capacitively loaded split pipes.[27] Their resonant frequencies and quality factors measured with the aid of a network analyzer of the type HP8753C were found as $\omega_0/(2\pi)$ =46.2±0.2 MHz and Q=105±5.

A single line of metamaterial elements is capable of propagating magnetoinductive waves in the passband around the resonant frequency. The dispersion equation of the MI waves for nearest neighbor interactions has the form[28,29]

$$1 - \frac{\omega_0^2}{\omega^2} - \frac{j}{Q} + \kappa_1 \cos kd = 0, \qquad (1)$$

where d is the separation between the elements, $k = \beta - j\alpha$ (β and α are the propagation and attenuation coefficients), κ_1 $= 2M_1/L$ is a coupling constant (L is the inductance of the
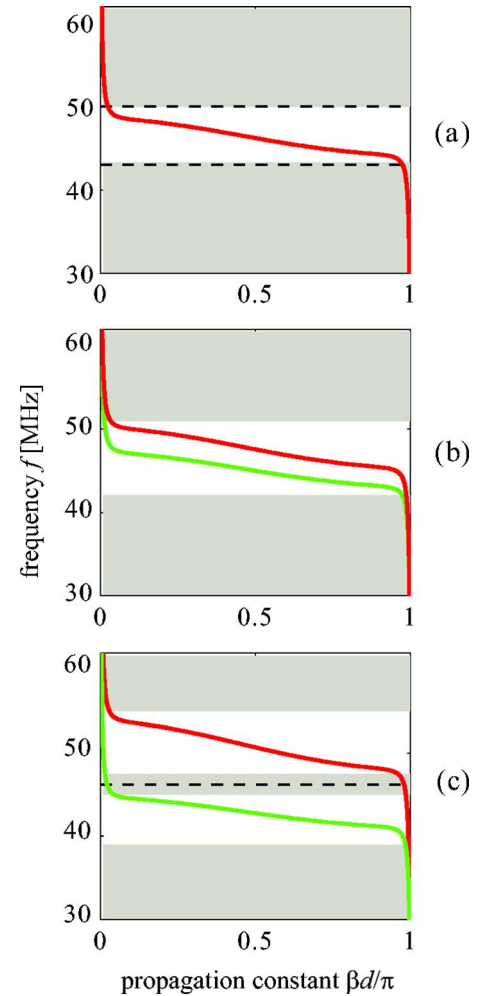

FIG. 2. (Color online) Dispersion characteristics of (a) an isolated line, (b) two coupled lines separated by h=20 mm, and (c) the same two lines separated by 10 mm. Stop bands preventing image spreading in the x direction are shown as gray areas. There are two stop bands for the single line (a). The separation between the stop bands is larger for two weakly coupled lines (b). An additional stop band around the resonant frequency (46.2 MHz) appears for the strongly coupled lines (c).

elements and M_1 is the mutual inductance between nearest neighbors in the same array).

In the case of two lines that are placed close enough to each other their elements are coupled not only to the elements of their own lines but also to the elements of the other line. As shown by Sydoruk *et al.*[27] two coupled one-dimensional lines of metamaterial elements, each one capable of propagating a magnetoinductive wave, form a "biatomic" metamaterial structure. A unit cell consists of two neighboring elements from each of the lines that are arranged axially and strongly interact with each other via the coupling constant $\kappa = 2M/L$, where M is now the mutual inductance between elements in the unit cell. The dispersion equation for two identical lines takes then the form[27]

$$\left(1 - \frac{\omega_0^2}{\omega^2} - \frac{j}{Q} + \kappa_1 \cos kd\right)^2 = \frac{\kappa^2}{4}. \qquad (2)$$

The dispersion curve for an isolated planar array is known to be in the form of a backward wave [see Fig. 2(a)]. If two planar lines are brought close to each other the dis-

persion curves retain their backward character but are split into an upper and lower branch. When the distance between the planar arrays is sufficiently small then the split may become so large that a stop band appears between the two backward wave regions. These split dispersion curves were found both experimentally and theoretically by Sydoruk *et al.*[27] for similarly arranged arrays. Examples for $h=20$ mm and $h=10$ mm are shown in Figs. 2(b) and 2(c). In the latter case there is a clear band gap around the resonant frequency which means that magnetoinductive wave propagation along each one of the lines is suppressed for any value of kd.

B. Near-field calculations

Our aim is to find the magnetic field in the image plane. For that we need to know the currents in each element. It would be possible to obtain approximate analytical solutions for the currents by following the approach employed in Ref. 27. We have, however, adopted here a more accurate alternative method which allows coupling between all N elements. The currents are then obtained numerically from the generalized Ohm's Law[26,29]

$$\mathbf{V} = \mathbf{ZI}, \tag{3}$$

where $\mathbf{Z}$ is the $N \times N$ impedance matrix, $Z_{ii}=j\omega L +1/(j\omega C)+R$, $i=1, 2, \ldots, N$; C and R are the capacitance and resistance of the loops; $Z_{ij}=j\omega M_{ij}$, $i=1, 2, \ldots, N$, $i \neq j$; M_{ij} is the mutual inductance between the ith and jth element. $\mathbf{I}$ and $\mathbf{V}$ are N-dimensional vectors of current and voltage. In our experimental arrangement each line consists of eleven elements thus the total number of elements considered is $N=23$ for the double and $N=12$ for the single lens, which includes the transmitter coil (assumed to have an additional resistance of $50~\Omega$ accounting for the effect of a $50~\Omega$ transmission line connecting the coil and the network analyzer in the experimental setup described later). The elements are not excited, except the transmitter which is assumed to have a voltage V_0 applied to it.

The currents are found by inverting the impedance matrix in Eq. (3). The total magnetic field in the image plane is then determined by summing up the contributions from the currents flowing in each one of the loops.

III. NEAR-FIELD LENS

In order to preserve the information given in the object plane we cannot allow the sideways (along the x axis) propagation of magnetoinductive waves. We may expect good imaging only in the stop band where the image of a subwavelength object, placed below the structure, can be translated to the top with only little distortion. To verify this prediction we performed a series of near field imaging experiments.

The spacing between the elements in the same line was $d=24$ mm. For the single lens the transmitting circular loop of 3 mm radius was placed at a distance 2.5 mm away from the line, and the magnetic field distribution in the imaging plane 2.5 mm above the line was scanned with the aid of the receiving loop of the same size (note that the size of both the transmitter and receiver loops is much smaller than that of the elements of the lens). The measurements were performed
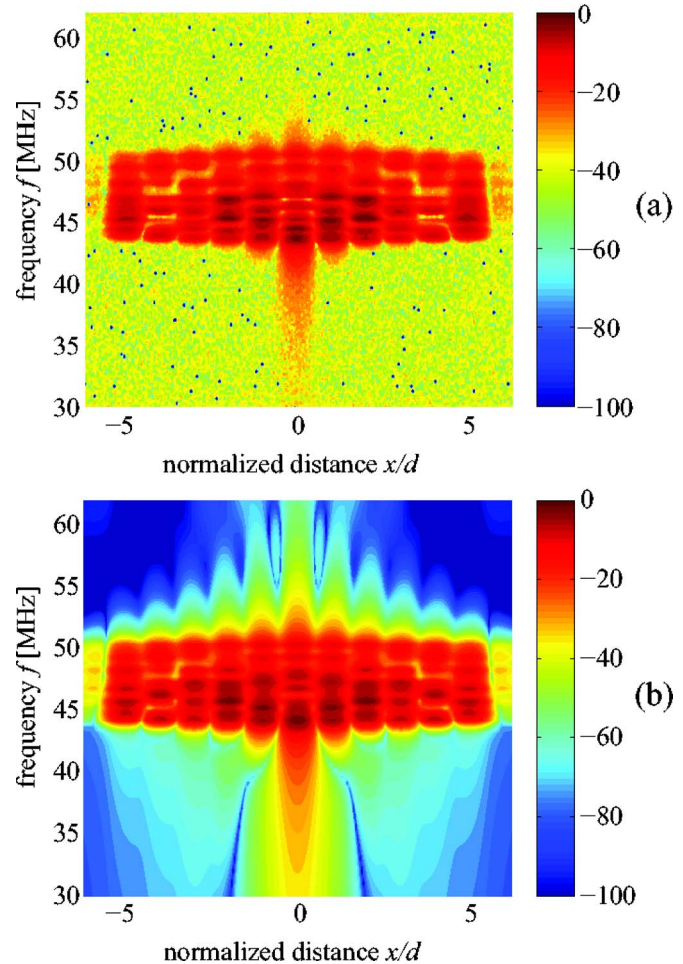

FIG. 3. (Color online) Near field imaging for the single lens. Magnetic field distribution in the image plane vs frequency (contour plot). Experiment (a) and theory (b).

at 1601 frequency points in the range of 30–62 MHz with the aid of a network analyzer HP8753ES connected to the transmitting and the receiving loop by a $50~\Omega$ transmission line. As the $50~\Omega$ loaded receiver is not matched to the analyzed structure,[30] the S_{21} parameter is proportional to the H_z component of the magnetic field (more details on this measurement setup are reported in Ref. 27).

For the double lens with the separation h between two lines the transmitter was placed at a distance $h/2$ below the bottom line, and the receiver scanned the magnetic field at a distance $h/2$ above the top line.

The experimentally obtained image field distribution as a function of frequency is shown for the single lens by the color coded contour plot of Fig. 3(a). Figures 4(a) and 5(a) show the same for the double lens for $h=20$ mm and $h =10$ mm. The corresponding theoretical plots are presented in Figs. 3(b), 4(b), and 5(b). The agreement between theory and experiment is remarkably good. For each configuration the experimental results reproduce all the details of the theoretical predictions. In fact, the only difference between theory and experiment is the signal amplitude in the stop bands. In the experimental plots they are green indicating the prevailing noise level of about 50 dB whereas in the theoret-
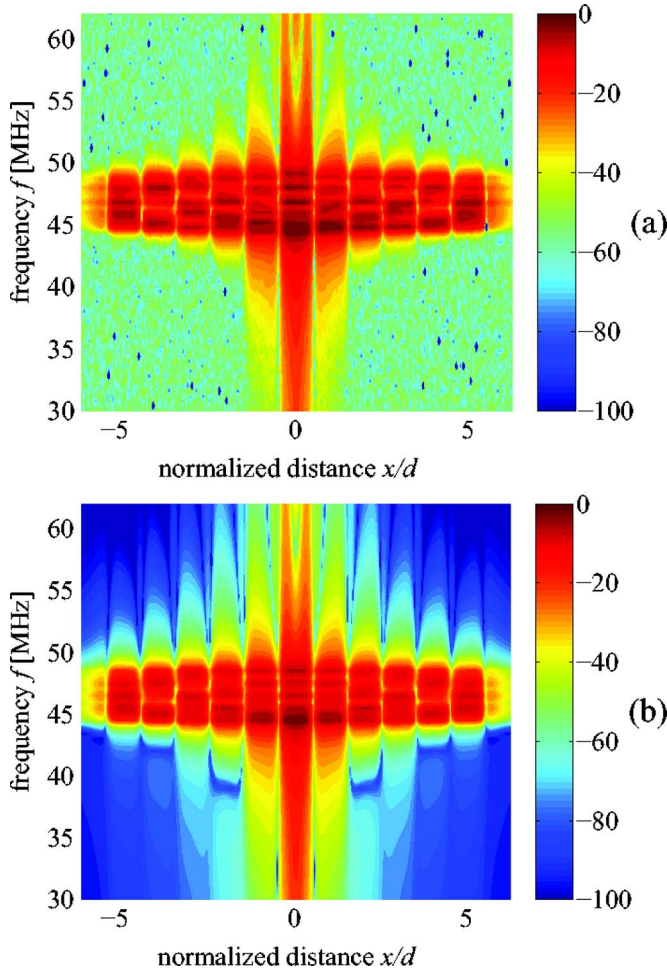
FIG. 4. (Color online) Near field imaging for the double lens with h =20 mm. Magnetic field distribution in the image plane vs frequency (contour plot). Experiment (a) and theory (b).

FIG. 5. (Color online) Near field imaging for the double lens with h =10 mm. Magnetic field distribution in the image plane vs frequency (contour plot). Experiment (a) and theory (b).

ical plots the signal level is shown by blue or deep blue indicating significantly lower values, as it should because noise is not included in the theory.

It may be seen in Figs. 3–5 that, as mentioned before, magnetoinductive waves may propagate in the passbands resulting in high magnetic fields at every element. One observes a broad field distribution corresponding to the excitation of the entire structure. There is a single passband in Fig. 3. The passbands may be seen to be overlapping in Fig. 4 since the lines are only weakly coupled [see Fig. 2(b)] whereas the passbands are clearly separated in Fig. 5 for the arrangement with strong coupling [see Fig. 2(c)].

If we wish to have a narrow image then we must use frequencies that are in one of the stop bands. As may be seen in Figs. 2(a)–2(c) there are two outer stop bands in Figs. 3 and 4 and an additional stop band in Fig. 5 in the vicinity of the resonant frequency. Since excitation in the outer stop bands is bound to be weak, the signal-to-noise ratio must suffer. Hence, the better candidate for successful imaging is the inner stop band.

The comparison between theoretical and experimental results shown in Fig. 5 by color coding offers an easily observable global picture. However, if we wish to see the details it is more informative to look at the curves at a single
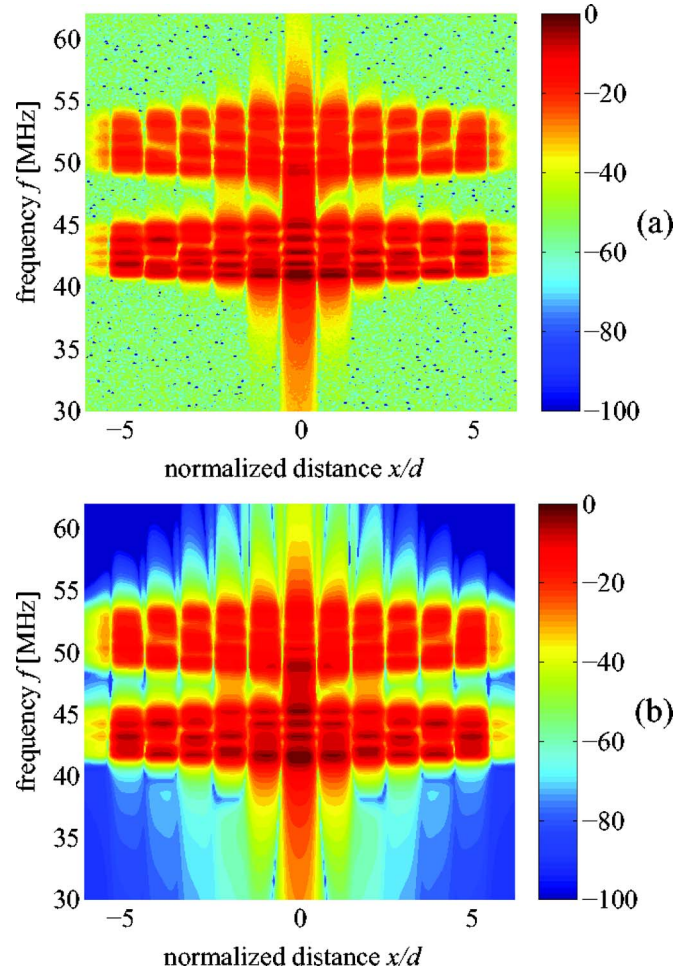
frequency. This is done in Fig. 6 where the comparison is for 46.2 MHz. There is excellent agreement between the theoretical (red) and experimental (blue crosses) results.

IV. COMPARISON BETWEEN A SINGLE LENS AND A DOUBLE LENS

Our conclusion so far is that the closely coupled double layer is better for imaging than the loosely coupled one and
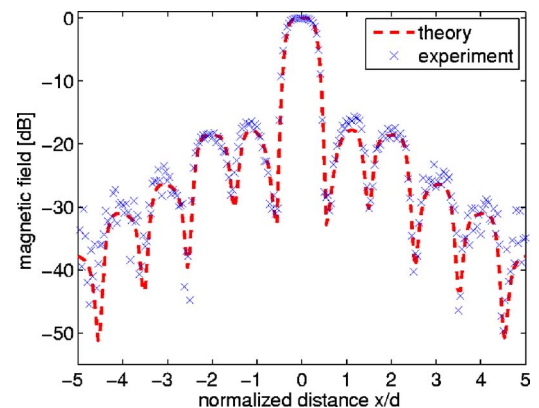

FIG. 6. (Color online) Theoretical (red curve) and experimental (blue crosses) magnetic field distribution in the image plane along the x axis for the double lens with h=10 mm separation at the resonant frequency (46.2 MHz).
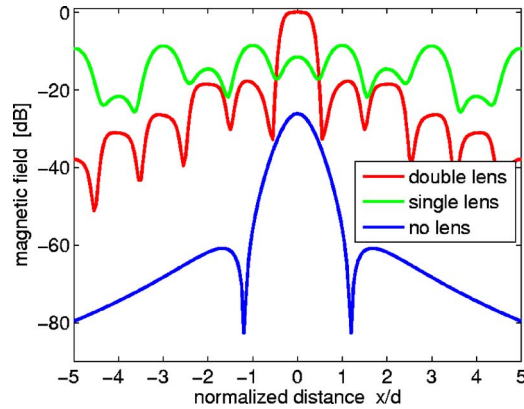
FIG. 7. (Color online) Theoretical magnetic field distributions along the *x* axis: double lens (red), single lens (green), in the absence of the lens (cyan). The frequency is 46.2 MHz. The image plane is 20 mm away from the transmitter in each case.

FIG. 8. (Color online) Theoretical magnetic field distributions along the *x* axis for the double lens at 46.2 MHz (red) and the single lens at 43 MHz (green) and 50 MHz (cyan). All three figures correspond to the frequencies in the stop bands of magnetoinductive waves [see Figs. 2(a) and 2(c), horizontal dashed lines within the stop bands].

the reason is the presence of a stop band around the resonant frequency for the former structure. Next we shall compare the single lens with the double lens. In order to make the comparison meaningful the positions of the transmitter and image plane for both cases remain at the same point, at $z = 0$ and $z = 20$ mm. The two layers of the double lens are at $z = 5$ mm and $z = 15$ mm, and the single lens (obtained by omitting one of the lines from the double lens) is assumed to be at $z = 10$ mm. The basis of the comparison is the distribution of the magnetic field along the *x* axis in the image plane.

In Fig. 7 three theoretical distributions are plotted at the resonant frequency of 46.2 MHz: (i) in the absence of a lens, i.e., the magnetic field of the transmitter coil, (ii) in the presence of a single lens, and (iii) in the presence of the double lens. The field is lowest in the absence of the lens. It is just the magnetic field distribution of the current carrying transmitter loop. In the presence of the single lens the field is higher everywhere but, as may be expected, it gives no imaging because due to the propagation of the magnetoinductive wave it is high over the whole region of interest. The ability of the double lens to image may be clearly seen. The amplitude is highest (normalized to 0 dB at the central peak) and there is no spread of the image. The next peak in the lateral direction is about 20 dB down.

Another comparison is shown in Fig. 8 where the magnetic field distribution in the image plane is plotted at three different frequencies where imaging occurs: (i) single lens in the lower stop band at 43 MHz, (ii) single lens in the upper stop band at 50 MHz, and (iii) the double lens at the resonant frequency of 46.21 MHz. It may be seen that in the stop bands of the single lens (green and blue curves) the imaging is quite good (the central peak is well distinguished from the secondary peaks) but the field amplitudes are much lower than for the double lens (red curve).

In Fig. 9 we show the theoretical distribution of the magnetic field along the *z* axis from $z = -10$ to $z = 30$ mm for four cases: the double lens at the resonant frequency, single lens at 43 and 50 MHz, and in the absence of a lens. The curves confirm the superior performance of the double lens. The amplitude in the image plane is highest for the double lens,
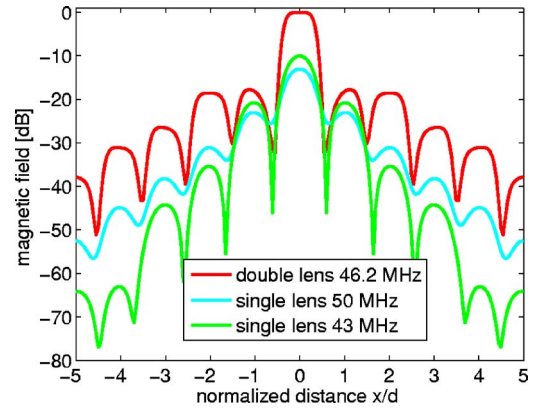
lower for the single lens and the lowest in the absence of the lens both at the output of the lens and at the image plane.

V. SUBWAVELENGTH IMAGING WITH A BILAYERED PLANAR METAMATERIAL

Having understood the imaging mechanism for a simple structure of two coupled lines we shall now apply our approach to a bilayered planar metamaterial called a "magnetoinductive lens" by Freire and Marques.[10] We choose a configuration with 542 elements being arranged in a honeycomb lattice with hexagonal boundaries in both layers as shown schematically in Fig. 10(a). Previously, a single-layered metamaterial of 271 hexagonally arranged Swiss rolls was investigated experimentally by Wiltshire *et al.*[6,22,24] and a model of its imaging mechanism considering magnetoinductive waves on coupled elements was described by Zhuromskyy *et al.*[26]

The dispersion characteristics $f(\beta_x, \beta_y)$ of a bilayered structure has two branches separated by a complete stop band if the layers are sufficiently close to each other, see Fig. 10(b). Taking the same parameters for the elements' geometry and for the lattice constant *d* as in Sec. II a clear sepa-
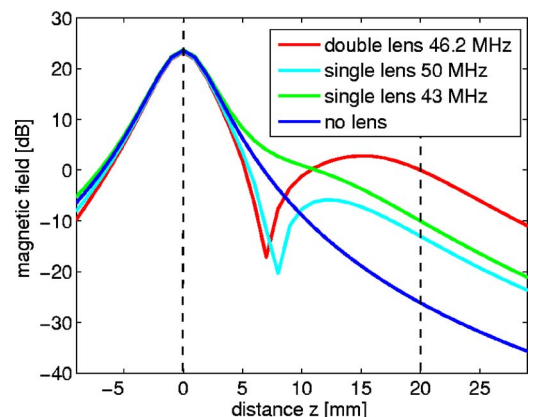

FIG. 9. (Color online) Theoretical magnetic field distributions along the *z* axis: double lens at 46.2 MHz (red), single lens at 43 MHz (green) and 50 MHz (cyan), and in the absence of lens (blue). The image plane is 20 mm away from the transmitter in each case as indicated by the dashed lines.
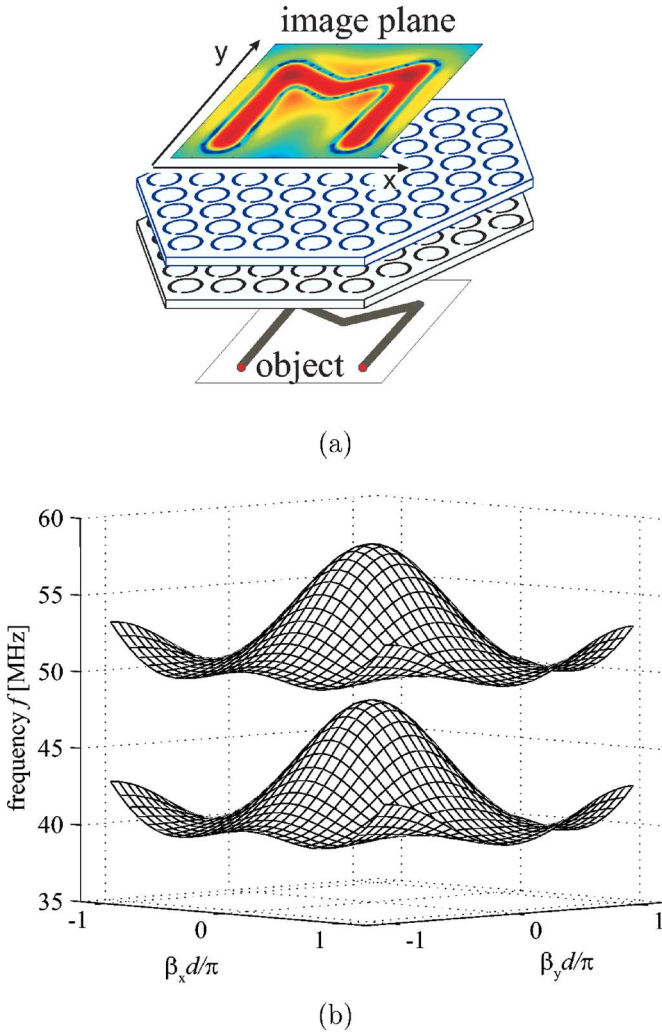
FIG. 10. (Color online) Bilayered magnetoinductive lens with hexagonally arranged elements. (a) The setup. (b) Dispersion surfaces $f(\beta_x, \beta_y)$ of magnetoinductive waves supported by the structure (nearest neighbor interactions, no losses).

FIG. 11. (Color online) Near field imaging with a bilayered planar structure. Magnetic field distribution at five frequencies $f_0 = 30$, 40, 49.3, 55.7, and 65 MHz (a)–(e). The distance between the object and image plane is 15 mm.

ration between the upper and the lower branch is achieved for the interlayer distance $h = 7.5$ mm, smaller than for the linear case considered in Secs. II–IV. The obvious reason is that in the planar metamaterial each element is surrounded by a larger number of neighbors within the same layer, so that stronger interlayer coupling is required to achieve a complete stop band. The corresponding single-branched dispersion of a single-layered metamaterial can be found in Fig. 2 of Ref. 26.

In the bilayered structure of Fig. 10 the stop bands permitting the pixel-to-pixel near field imaging lie at $f < 39.3$ MHz, $48 <$ MHz $f < 49.6$ MHz, and $f > 58.2$ MHz. Figure 11 shows the image calculated from a model taking all interactions into account for five frequencies, corresponding to the lower outer stop band (a), to the lower passband (b), to the inner stop band (c), to the upper passband (d) and to the upper outer stop band (e). Just as in the simpler case of the linear lens, imaging may be seen to be possible only in the stop bands (a), (c), and (e) whereas in both passbands the image appears distorted due to the excitation of magnetoinductive waves. The signal in the inner stop band is 20 dB
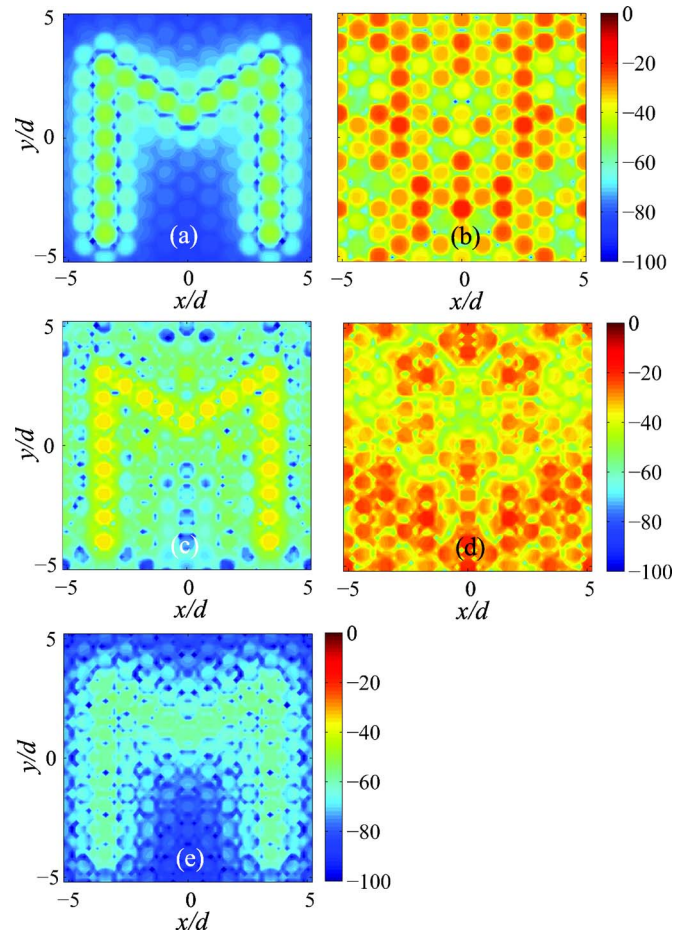
larger than in outer stop bands which will be crucial in a practical device where a signal well above noise level is needed.

In Fig. 12 we compare the distribution of the magnetic field along the z axis from $z = -7.5$ to $z = 30$ mm for four cases: the double planar lens at 49.2 MHz, single planar lens
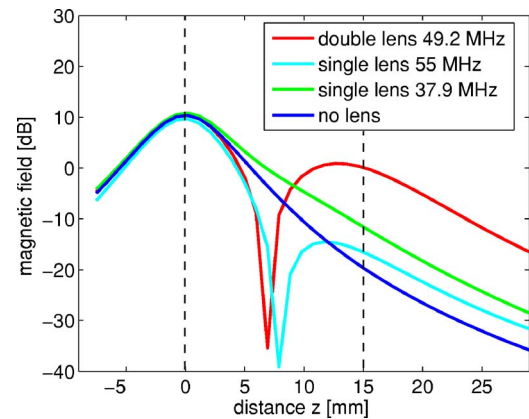

FIG. 12. (Color online) Theoretical magnetic field distributions along the z axis for the hexagonal metamaterial: double lens at 49.2 MHz (red), single lens at 37.9 MHz (green) and 55 MHz (cyan), and in the absence of lens (blue). The image plane is 15 mm away from the transmitter in each case as indicated by the dashed lines.

at 37.9 and 55 MHz, and in the absence of a lens, where the excitation is in the form of a small loop of 5 mm radius. Analogous to the simpler case of a linear lens (Fig. 9) the curves confirm the superior performance of the bilayered planar metamaterial. The amplitude is the highest for the bilayered structure; it is lower for the single-layer-structure and the lowest in the absence of the lens both at the output of the lens and in the image plane. The strong magnetic field at the output of the double lens (Figs. 9 and 12) is attributed to its rear-surface resonance.[2,7] The magnetic field declines in both directions from the surface. Therefore, inside the lens, in the vicinity of the rear surface, the magnetic field appears to grow in the forward direction.[1,7,10]

VI. CONCLUSIONS

A theoretical and experimental study of a subwavelength lens consisting of one or two one-dimensional layers of magnetic metamaterial elements has been presented. It has been shown that in order to achieve imaging the transverse propagation of magnetoinductive waves must be suppressed. In the general case this may happen in the stop bands of the dispersion characteristics. The best image may be obtained when the two arrays are strongly coupled leading to a stop band in the vicinity of the resonant frequency. The imaging capabilities of double (consisting of two layers) and single (consisting of one layer) lenses have been compared and it has been shown that the achievable signal levels are higher for the double lens. Excellent agreement between experimental and theoretical results has been demonstrated for linear arrays of 22 elements. It has further been demonstrated that the same mechanism is responsible for the image formation in bilayered planar metamaterials consisting of 542 elements. The resolution has been shown to be related to element size. Thus a search for smaller low frequency resonators could lead to further improvement in resolution.

ACKNOWLEDGMENTS

[1] J. B. Pendry, Phys. Rev. Lett. **85**, 3966 (2000).
[2] E. Shamonina, V. A. Kalinin, K. H. Ringhofer, and L. Solymar, Electron. Lett. **37**, 1243 (2001).
[3] D. O. S. Melville and R. J. Blaikie, J. Opt. Soc. Am. B **23**, 461 (2006).
[4] E. Shamonina and L. Solymar, Progress in Electromagnetics Research Symposium PIERS 2002, Cambridge, MA, 2002.
[5] D. Korobkin, Y. Urzhumov, and G. Shvets, J. Opt. Soc. Am. B **23**, 468 (2006).
[6] M. C. K. Wiltshire, J. B. Pendry, I. R. Young, J. Larkman, D. J. Gilderdale, and J. V. Hajnal, Science **291**, 849 (2001).
[7] S. Maslovski, S. Tretyakov, and P. Alitalo, J. Appl. Phys. **96**, 1293 (2004).
[8] P. A. Belov, C. R. Simovski, and P. Ikonen, Phys. Rev. B **71**, 193105 (2005).
[9] S. Maslovski and S. Tretyakov, J. Appl. Phys. **94**, 4241 (2003).
[10] M. J. Freire and R. Marques, Appl. Phys. Lett. **86**, 182505 (2005).
[11] C. A. Allen, K. M. K. H. Leong, and T. Itoh, IEEE MTT-S Int. Microwave Symp. Dig. **3**, 1875 (2003).
[12] I.-H. Lin, C. Caloz, and T. Itoh, Microw. Opt. Technol. Lett. **44**, 416 (2005).
[13] R. Silin, Izv. Vyssh. Uchebn. Zaved., Radiofiz. **15**, 809 (1972).
[14] R. A. Silin, Opt. Spectrosc. **44**, 189 (1978).
[15] R. A. Silin, *Periodic Waveguides* (Phasis, Moscow, 2002) (in Russian).
[16] R. Zengerle, J. Mod. Opt. **34**, 1589 (1987).
[17] D. R. Smith, D. Schurig, J. J. Mock, P. Kolinko, and P. Rye, Appl. Phys. Lett. **84**, 2244 (2004).
[18] D. N. Chigrin, S. Enoch, C. M. S. Torres, and G. Tayeb, Opt. Express **11**, 1203 (2003).
[19] H.-T. Chien, H.-T. Tang, C.-H. Kuo, C.-C. Chen, and Z. Ye, Phys. Rev. B **70**, 113101 (2004).
[20] Z.-Y. Li and L.-L. Lin, Phys. Rev. B **68**, 245110 (2003).
[21] C.-H. Kuo and Z. Ye, Phys. Rev. E **70**, 056608 (2004).
[22] M. C. K. Wiltshire, J. V. Hajnal, J. B. Pendry, D. J. Edwards, and C. J. Stevens, Opt. Express **11**, 709 (2003).
[23] P. A. Belov, Y. Hao, and S. Sudhakaran, Phys. Rev. B **73**, 033108 (2006).
[24] M. C. K. Wiltshire, J. V. Hajnal, J. B. Pendry, and D. J. Edwards, *Proceedings of the 27th ESA Antenna Technology Workshop on Innovative Periodic Antennas: Electromagnetic Bandgap, Left-handed Materials, Fractal and Frequency Selective Surfaces* (ESA Publications Division, Noordwijk, The Netherlands, 2004).
[25] J. N. Gollub, D. R. Smith, D. C. Vier, T. Perram, and J. J. Mock, Phys. Rev. B **71**, 195402 (2005).
[26] O. Zhuromskyy, E. Shamonina, and L. Solymar, Opt. Express **13**, 9299 (2005).
[27] O. Sydoruk *et al.*, Phys. Rev. B **73**, 224406 (2006).
[28] E. Shamonina, V. A. Kalinin, K. H. Ringhofer, and L. Solymar, Electron. Lett. **38**, 371 (2002).
[29] E. Shamonina, V. A. Kalinin, K. H. Ringhofer, and L. Solymar, J. Appl. Phys. **92**, 6252 (2002).
[30] F. Mesa, M. J. Freire, R. Marques, and J. D. Baena, Phys. Rev. B **72**, 235117 (2005).